DOI:10.1190/image2022-3745686.1

DAS noise attenuation using wavelet stack

Zhou Yu, Zhaojun Liu, Ge Zhan, Peng Cheng, Bin Wang, TGS, Houston, USA. Weihong Fei, Chevron*

Summary

Dense spatial sampling (~1m) and low signal-to-noise ratio (SNR) are typical features of distributed acoustic sensing (DAS) data. We have developed a wavelet stacking method to attenuate DAS noise without compromising data bandwidth. Wavelet stack consists of two steps, adaptive nonlinear iterative denoise and nonlinear stack. Nonlinear iterative filtering is based on combination of 1D stationary wavelet transform, 2D complex wavelet transform (CWT) and normal moveout. It is non-stationary and adaptive to noise variation. Nonlinear stack combines two denoised gathers in the CWT domain in a predictable way for further SNR uplift without loss of the high frequency information of either input. Wavelet stack is used to produce partially stacked DAS channel gathers. Significant seismic resolution uplift in field DAS data is demonstrated using the newly developed wavelet stack compared to a conventional linear stack.

Introduction

Distributed acoustic sensing (DAS) has been popular to the exploration industry for its cost effective and novel way of turning the fiber-optic cable into a large seismic array (e.g., Zhan et. al., 2016), which can provide valuable imaging and monitoring of fluid and pressure variations in the reservoir. Nowadays, more and more DAS VSP data are acquired on actively producing and injecting wellbores at a lower cost and without well intervention. However, downhole production or injection activities inevitably become noise sources, which travel along the wellbore and usually don't contain any useful subsurface information. It is the noise for reflection seismology and can significantly degrade the quality of the image. This noise is high amplitude and broadband in the frequency or wavenumber domain. Additional challenges are strong variation of noise characteristics and spatial aliasing. Conventional methods, like deconvolution or Fourier transform based methods are less effective in addressing these noise problems because of the stationary statistics assumption and presence of aliased energy in the data (e.g., Yu et. al., 2002; Yu and Garossino, 2004). Therefore, can we find an adaptive denoise workflow requiring minimum human interference to maximize SNR while keeping data bandwidth?

Geophone arrays have been widely used in the industry to suppress the horizontal traveling waves by linear stacking to gain better SNR (e.g., Graig and Genter, 2006). Regone (1998) proposed Chebychev-weighted areal geophone arrays based on SNR ratios by applying a series of array filters with known attenuation levels to the raw data. Unlike surface seismic acquisition, DAS fibers are typically installed in boreholes, either cemented behind the casing or clamped on the production tubing. Therefore, there is no such flexibility to design the geophone array (e.g., Li, et. al., 2013) to reduce direct arrival or waves traveling along wellbore which carry no information of subsurface we are interested in.

Simple linear summation over the designed geophone array or any shape patch array has shown effective noise suppression (Craig and Genter, 2006), Similarly, a conventional way of reducing data volume prior to migration is to stack adjacent traces to generate a super trace. Mathematically speaking, linear stack is a lowpass filter and some high frequency information may be compromised (Jackson, 1989). Can we find a way to produce the super gather that has a similar or better SNR uplift to linear stack, but without compromising high frequencies?

A fusion methodology integrates multiple images of one object from different sensors into a single composite image that preserves all the significant features of each input image (Pajares., et. al., 2004). One of the widely used fusion methods is multiresolution wavelet decomposition-based scheme (e.g., Zhang and Blum, 1999). It shows that a simple nonlinear operation in the wavelet transform domain can combine diverse features from various sensors to produce enhanced temporal and spatial characteristics in the fused image. Can we apply the strategy of wavelet multi-resolution fusion technology to multi-sensor seismic data and reduce the data volume without compromising the resolution?

In this paper, we first discuss the wavelet stack workflow and its two components: the nonlinear adaptive denoise workflow and the nonlinear stack. The stationary wavelet and complex wavelet transforms are then briefly reviewed so that the amplitude threshold filtering function can be introduced. The 3rd part discusses the procedure of the wavelet nonlinear stack and the conditions applied for better SNR without sacrificing data bandwidth. Finally, we demonstrate the effectiveness of this nonlinear denoise and stack method with field data examples and conclude with a discussion of some of the practical issues involved.

Wavelet stack

Finer sensor spacing in DAS acquisition is common because there is no additional cost (e.g., Li, et. al., 2013; Zhan et. al., 2020). However, this high-density data may be not transformed to a high-quality image because of oversampling and limited aperture. It is common practice to

decimate the raw data volume by linear stacking over adjacent traces to gain a better SNR while reducing the volume of data for migration (e.g., Yu and Zhan, 2017; Zhan and Nahm, 2020). Independent recordings on adjacent receivers have been verified by varying the noise pattern and near-offset signals. Therefore, SNR improvement from the linear stack process is real. Significant noise has been observed in the data, coming from the production, casing ringing, random acoustic bursts, and nearby undesired acoustic sources. Next, we are going to discuss the two-step wavelet stack workflow: (1) a nonlinear iterative denoise workflow and (2) nonlinear combination of two input data in the CWT domain, to maximize SNR while preserving data bandwidth.

The nonlinear iterative denoise workflow

We prefer to model seismic data as nonstationary time and space wavefields and to use the local time-space domain as well as the frequency-wavenumber characteristics to design appropriate filters. We separate the signal from the noise in a multidimensional space created by a 1D or 2D wavelet transform. Normal moveout (NMO) is used to increase the dip differences between reflections and other unwanted energy (Yu et. al., 2017). 1D wavelet transform based filtering targets low frequency, outlier amplitude noise which could degrade the effectiveness of 2D filtering. An ideal noise attenuation technique should handle the variation in noise characteristics from shot to shot or receiver to receiver in a completely adaptive and automatic way.

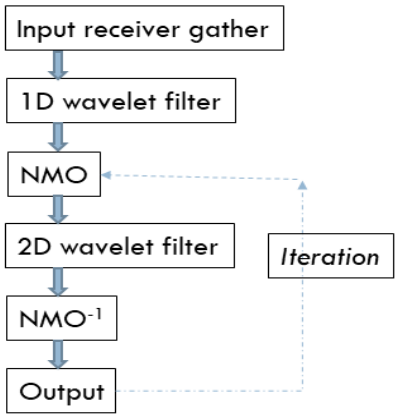

Figure 1: Nonlinear and iterative denoise workflow.

The procedure for amplitude threshold filtering in the wavelet transform domain involves the same three steps as filtering in other transform domains. First, the data are decomposed into wavelet space by wavelet transformation. Then, the portions of the data to be removed are identified and excluded from the inverse transform, which reconstructs the original data, but modified by the filter operation. We define the forward wavelet transform as $\boldsymbol{W}$, the inverse wavelet transform $\boldsymbol{W}^{-1}$, input data $\boldsymbol{D}$ and threshold filter function $\boldsymbol{T}$, 1D or 2D filter procedure in Figure 1 can be expressed as

$$\boldsymbol{D}' = \boldsymbol{W}^{-1}\{\boldsymbol{T}\boldsymbol{W}(\boldsymbol{D})\} \qquad (1)$$

where $\boldsymbol{D}$' is filtered result. For 1D wavelet filtering, W represents the stationary wavelet transform to avoid phase distortion introduced by the decimation at each scale in a standard discrete wavelet transform. For a more detailed discussion and the potential artifacts introduced during seismic filtering applications, see Yu and Whitcombe (2009) and Yu and Garossino (2004). The hreshold filter function T is defined as

$$\boldsymbol{T} = \begin{cases} 0 \ when \ \boldsymbol{W}(\boldsymbol{D}) > \boldsymbol{\theta} \\ 1 \ when \ \boldsymbol{W}(\boldsymbol{D}) \leq \boldsymbol{\theta} \end{cases} \qquad (2)$$

where $\boldsymbol{\theta}$ is the wavelet coefficient threshold and a function of scale and time. Here $\boldsymbol{T}$ truncates amplitudes greater than θ regardless of their scale and temporal position. For a more detailed discussion of T, please see Yu et. al. (2002).

Effective suppression of noise requires a stable and robust difference between primary signal and the noise. 1D wavelet filtering has limitations; it doesn't consider the spatial continuity of reflections and is less effective when dip is the main distinguisher. Of various kinds of multi-scale and multi-orientation higher dimensional wavelet transform, we have selected the 2D complex wavelet transform (CWT) (Kinsbury, 1999; Yu and Whitcombe, 2008; Yu et. al., 2017).

CWT is also called dual-tree complex wavelet transform, which is a complex-value extension of the discrete wavelet transform. It uses complex-valued filtering that decomposes the real signals into real and imaginary parts in the transform domain. The real and imaginary coefficients satisfy the Hilbert relation and are used to compute amplitude and local phase information. It has limited redundancy, which is independent of the number of scales (4:1 for 2D). This buys us the important property of translation-invariance, while requiring a relatively small memory compared to those in un-decimated forms. The run time varies as $4N^2$, which is faster than $(NlogN)^2$ for 2D FFT (with N x N input array). Since no global transform (such as the Fourier transform) is involved, the CWT doesn't spread the aliased energy, even if the input data contains aliasing. Finally, orientations, +75, +45, +15 degree, at each scale (Figure 2) in CWT provide good directionality. The smooth variation in its amplitude for each orientation (3rd row of Figure 2) suggests the CWT overcomes the checkerboard artifacts of the discrete wavelet transform (e.g., Yu and Whitcombe, 2009; Yu et. al., 2017).

For the 2D wavelet filter in our nonlinear iterative denoise workflow (Figure 1), $\boldsymbol{W}$ and $\boldsymbol{W}^{-1}$ in equation (1) represent forward and inverse 2D CWT respectively. $\boldsymbol{T}$ in equation (1) is replaced by $\boldsymbol{T}'$, which defined as

$$\boldsymbol{T}' = \begin{cases} 1 & when\ \boldsymbol{W}(\boldsymbol{D})(\boldsymbol{t},\boldsymbol{x},\boldsymbol{s},\boldsymbol{o},\boldsymbol{r}) \in \boldsymbol{\theta}' \\ 0 & otherwise \end{cases} \qquad (3)$$

where $\boldsymbol{\theta}'$ is signal set and data dependent. The 2D CWT transforms 2D input **D** ($\boldsymbol{t}$, $\boldsymbol{x}$) into a 5D array in the 2D CWT domain, in which vectors of **t**, **x**, **s** and **o** are time, space, scale and orientation respectively. **r** represents two components of real and imaginary parts. We will discuss how to determine $\boldsymbol{T}'$ and $\boldsymbol{\theta}'$ in the field data example section.

The filter iterates (Figure 1) by the output of the 1st run becoming the input to the 2nd run, starting at NMO as indicated by the dashed line in Figure 1. The 1D wavelet filter is not included in the iterative process.

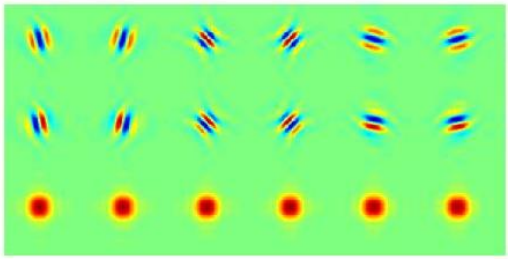

Figure 2: Complex wavelet basis. Orientations from left to right are -/+75, -/+45 and -/+15 degrees respectively. The top row is real, the middle row is imaginary and the bottom one is amplitude.

Wavelet nonlinear stack

The goal is to achieve a similar or better SNR as that of a linear stack without losing high frequency information.

Wavelet stack transforms two input gathers to the CWT domain, and then combines two coefficients at each position in the CWT domain with the combined energy at the selected scales. matching the bigger one of the two inputs. The final step is to apply the inverse CWT to the combined coefficients. Suppose we have two input gathers, D1 and D2 and their CWT counterparts, $\mathbf{C}^1$(**t**,**x**,**s**,**o**,**r**) and $\mathbf{C}^2$(**t**,**x**,**s**,**o**,**r**), a simple summation in the CWT domain is:

$$\boldsymbol{C}^{12}(t,x,s,o,r) = 0.5 * (C^2 1(t,x,s,o,r) + C^1(t,x,s,o,r)) \qquad (4)$$

where **t**, **x**, **s**, **o** and **r** are vectors and represent two dimensional variables, scale, orientation and the real or imaginary part respectively. Since CWT is a linear transform (Mallat, 1999), the inverse CWT of $\mathbf{C}^{12}$ equals the result of linear stack if no additional step is applied to $\mathbf{C}^{12}$. After SNR is gained in equation (4), we will apply following to $\mathbf{C}^{12}$ in the selected scales, s', a subset of scale vector $\boldsymbol{s}$, before the inverse CWT is applied.

$$C_{s'}{}^{12} = f_{s'} C^{12} \qquad (5)$$

Where $f_{s'}$ is a scaling factor applied to all coefficients at scale s' and determined by

$$f_{s'} = sqrt\left\{\frac{Q_{s'}}{\sum_{s'}\left(C^{12}(s')\right)^2}\right\} \qquad (6)$$

where $\sum_{s'}$ represents summation of coefficients at a given s' regardless of other axes and $Q_{s'}$ is

$$Q_{s'} = \max\left(\sum_{s'}\left(C^1(s')\right)^2, \sum_{s'}\left(C^2(s')\right)^2\right) \qquad (7)$$

For a given scale s', $Q_{s'}$ is a bigger value of energy summation of coefficients between C^1 and C^2. Therefore, $f_{s'}$ is always greater or equal to 1. Operation (5) assures no high frequency loss after combination of two input gathers when selected scale s' are normally scales 1 and 2 depending on input data bandwidth.

Field data example

Consider the two DAS field data common receiver gathers shown in Figure 3a. We see significant production and pump noise and a hint primary reflection. We apply the first iteration of our denoise workflow (Figure 1) using a constant NMO velocity of 6500 ft/s; T in equation 2 zeros coefficients greater than mean value of scale 5 and above; T' in equation 3 zeros everything at scale 1 and orientations +/-75 degrees. The result (Figure 3b) shows a huge noise reduction and clear hyperbolic primary events with no visible signal leakage in difference (Figure 3c). Spectral comparison (Figure 3d) demonstrates that the data characteristics and bandwidth are preserved in the filtered result, while strong low frequency production noise is suppressed.

We further examine the result in common shot domain (Figure 4). Strong, long wavelength noise makes reflection signal almost invisible (Figure 4a). It is very difficult to separate the signal from noise in the shot domain because of a lack of clear and simple differences between them. After denoise in the common receiver domain (Figure 4b), SNR is dramatically improved, and the highlighted signals are revealed, and no damage of the signal is observed on the difference (Figure 4c).

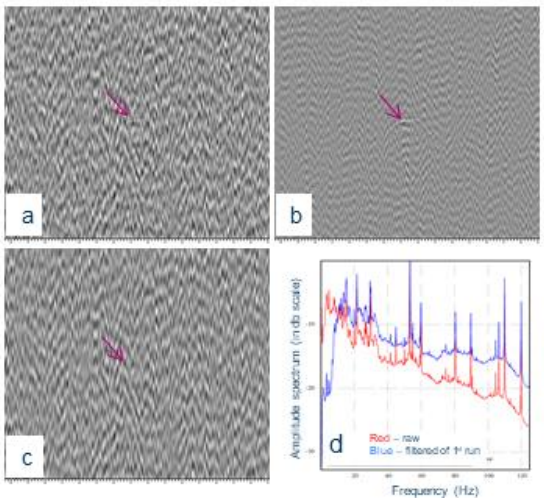

Figure 3: (a) is two raw DAS receiver gathers. (b) is the result of nonlinear filtering in Figure 1. (c) is the difference between (a) and (b). (d) is spectrum comparison of input (a) and the result (b).

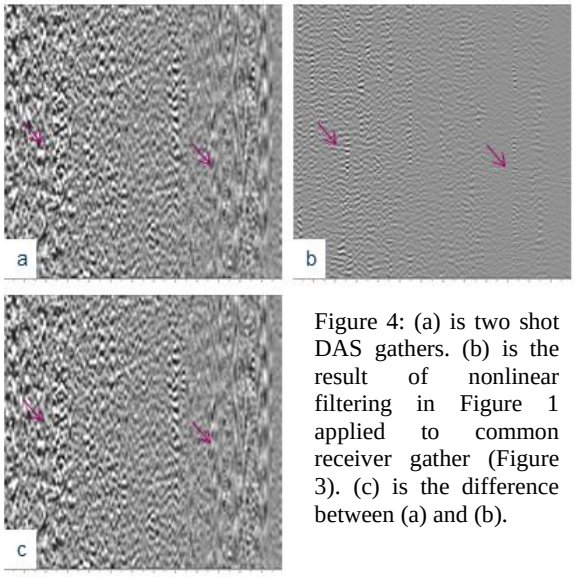

Figure 4: (a) is two shot DAS gathers. (b) is the result of nonlinear filtering in Figure 1 applied to common receiver gather (Figure 3). (c) is the difference between (a) and (b).

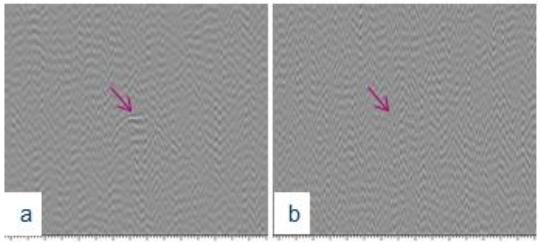

Figure 5: (a) is result of the iterated filtering of Figure 1 with input Figure 3b. (b) is the difference between input (Figure 3b) and the iterative result (a).

The iterative filtering in Figure 1 is then performed using the initial filtered result (Figure 3b) as an input to the 2D CWT filter. The threshold filter function T in equation 3 now zeros all coefficients on both scales 1 and 2 for +/-75 degree dips. The result (Figure 5a) shows further noise energy reduction, and no is signal found in the removed energy (Figure 5b).

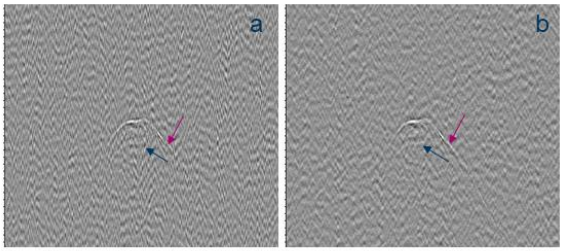

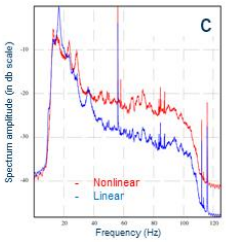

Figure 6: (a) is linear stack. (b) is wavelet stack via CWT. (c) is the spectrum comparison of (a) and (b).

After nonlinear denoise (Figure 1), we have examined linear vs wavelet stack over a radius of 5m or neighboring 10 receiver gathers. Compared to linear stack (Figure 6a), better SNR is clearly observed on the wavelet stack result (figure 6b). The primary events highlighted by the dark blue and dark pink pointers are better identified in the wavelet stack (Figure 6b) than in the linear stack (Figure 6a). The spectral analysis (Figure 6c) confirms the aim that wavelet stack (red curve) has better high-frequency preservation.

Discussion and conclusion

We are confident to say yes to three questions posted in the introduction, SNR improvement without compromising bandwidth, finding a new way of stack than linear one for preserving high frequencies while keeping SNR, and wavelet multiresolution fusion strategy for integrating multiple seismic sensor images. The nonlinear, non-stationary and multi-dimensional denoise workflow is integral part of wavelet stack. Field data examples have demonstrated the effectiveness of wavelet stack in SNR improvement and data bandwidth preservation over the conventional method.

Acknowledgements

We thank TGS for permission to publish this work. The authors thank Chevron for permission to publish the DAS field data and results. The authors also thank Sarah Spoors for reviewing the paper

REFERENCES

Craig, M. S., and R. Genter, 2006, Geophone array formation and semblance evaluation: Geophysics, **71**, no.1, Q1–Q8, doi: https://doi.org/10.1190/1.2159055.

Jackson, L. B., 1989, Signal filters and signal processing, 2nd ed.: Kluwer Academic Publishers, 49–52.

Kinsbury, N.G., 1999, Shift invariant properties of the dual-tree complex wavelet transform: Processing of the IEEE Conference on Acousics, Speech and Signal Processing, 16–19.

Li, Q., B. Hornby and J. Konkler, 2013, A permanent borehole fiber-optic distributed acoustic sensing experiment: 83rd Annual International Meeting, SEG, Expanded Abstract, 5057–5061, doi: https://doi.org/10.1190/segam2013-0698.1.

Mallat, S., 1999, A wavelet tour of signal processing: Academic Press.

Pajares, G. and J. Cruz, 2004, A wavelet-based image fusion tutorial: Pattern Recognition, **37**, 1855–1872 doi: https://doi.org/10.1016/j.patcog.2004.03.010.

Regone, C. J., 1998, Suppression of coherent noise in 3-D seismology: The Leading Edge, **17**, 1584–1589, doi: https://doi.org/10.1190/1.1437900.

Yu, Z., R. Abma, J. Etgen and C. Sullivan, 2017, Attenuation of noise and simultaneous source interference using wavelet denoising: Geophysics, **82**, no. 3, V179–V190, doi: https://doi.org/10.1190/geo2016-0240.1.

Yu, Z., and P. G. A. Garossino, 2005, High-energy noise attenuation of seismic data in the wavelet-transform domain: Integrated Computer-Aided Engineering, **12**, 57–67, doi: https://doi.org/10.3233/ICA-2005-12105.

Yu, Z., G. McMechan, P. Anno, and J. Ferguson, 2002, Adaptive wavelet filtering of seismic data in wavelet transform domain: Journal of Seismic Exploration, **11**, 223–246.

Yu, Z., G. McMechan, P. Anno, and J. Ferguson, 2007, Wavelet-Radon domain dealiasing and interpolation of seismic data: Geophysics, **72**, no. 2, V41–V49, doi: https://doi.org/10.1190/1.2422797.

Yu, Z., and D. Whitcombe, 2008, Seismic noise attenuation using 2D complex wavelet transform: 70th Annual International Conference and Exhibition, EAGE, Extended Abstracts, H015, doi: https://doi.org/10.3997/2214-4609.20147772.

Yu, Z., and D. Whitcombe, 2009, Potential timing shift errors when using the discrete wavelet transform with seismic data processing: 79th Annual International Meeting, SEG, Expanded Abstracts, 3218–3222, doi: https://doi.org/10.1190/1.3255526.

Yu, Z., and G. Zhan, 2017, VSP and DAS data noise attenuation using complex wavelet transform: 87th Annual International Meeting, SEG, Expanded Abstracts, 5999–6002, doi: https://doi.org/10.1190/segam2017-17642809.1.

Zhan, G., J. Kommedal, and J. Nahm, 2016, VSP field trials of distributed acoustic sensing in Trinidad and Gulf of Mexico: 86th Annual International Meeting, SEG, Expanded Abstracts, 5539–5543, doi: https://doi.org/10.1190/segam2015-5876420.1.

Zhan, G., J. Paul Gestel and R. Johnston, 2020, DAS data recorded by a subsea umbilical cable at Atlantis field: 90th Annual International Meeting, SEG, Expanded Abstracts, 510–514, doi: https://doi.org/10.1190/segam2020-3427669.1.

Zhang, Z., and R.S. Blum, 1999, A categorization of multiscale-decomposition-based image fusion schemes with a performance study for a digital camera application: Proceedings of the IEEE, **87**, 1315–1326 doi: https://doi.org/10.1109/5.775414.